

New Limits on Gravitational Radiation using Pulsars

A. N. Lommen

Astronomy Department & Radio Astronomy Laboratory, University of California, Berkeley, CA 94720-3411, USA
 currently at Sterrenkundig Instituut, University van Amsterdam, Kruislaan 403, 1098 SJ Amsterdam, the Netherlands
 email: alommen@astro.uva.nl

Abstract. We calculate a new gravitational wave background limit using timing residuals from PSRs J1713+0747, B1855+09, and B1937+21. The new limit is based on 17 years of continuous data pieced together from 3 different observing projects: 2 at the Arecibo Observatory and 1 at the 140ft Green Bank Telescope. This project represents the earliest results from the ‘Pulsar Timing Array’ which will soon be able detect the stochastic background from early massive black hole mergers.

European and Australian telescopes to maximize the observation time and the range of observations available.

Pulsar timing residuals are sensitive to gravitational radiation of wavelengths of about 1 yr, making the PTA complementary to LISA which will measure much shorter wavelengths, and the pCMBR which will measure much longer wavelengths.

Using timing residuals from Arecibo Observatory observations of PSRs B1937+21 and B1855+09 over 8 yr, Kaspi, Taylor, & Ryba (1994, hereafter KTR94) placed a limit of

$$\Omega_g h^2 < 6 \times 10^{-8} \quad (95\% \text{ confidence})$$

1. Introduction

There are two categories of sources that could produce a detectable level of stochastic gravitational radiation from the distant Universe. One is of cosmological origin and the other involves galaxy evolution. First, low-frequency (10^{-20} to 0 Hz) relic gravitational radiation may be generated during inflation, according to string theory models of the early Universe, via both early evolution of the extra dimensions and decay of cosmic strings. Cosmic strings, while now disfavored as the driver behind structure formation in the Universe, still arise in many grand unified theories of particle physics after the epoch of inflation (Caldwell, Kamionkowski, & Wadley 1998; Hogan 2000; see also Maggiore 2000). Second, the coalescence of massive black holes (MBHs) during galaxy evolution could also produce a detectable level of Gravitational Waves (GWs). (See Lommen & Backer 2001 for more on this.) Three cosmology experiments are being conducted or planned by a number of investigators around the globe to either detect or place new limits on the stochastic background of gravitational radiation: polarization of the Cosmic Microwave Background Radiation (pCMBR), Pulsar Timing Array (PTA), and Laser Interferometer Space Array (LISA).

The PTA consists of a regular observing schedule on a handful of the millisecond pulsars that are most accurate as clocks. So far, we have used the Arecibo Telescope in conjunction with the Green Bank 140ft telescope, but we plan on including the new Green Bank 100-m telescope that has just been commissioned and a collection of other

where Ω_g is the fractional energy density in gravitational waves per logarithmic frequency interval and the Hubble constant $H_o = 100h \text{ km s}^{-1} \text{ Mpc}^{-1}$. We have connected the KTR94 data to 10 years of Green Bank 140ft telescope data and 3 years of Arecibo Observatory data. The overlapping data sets span a total of nearly 17 years, doubling the baseline of Kaspi et al’s results. The sensitivity of the PTA is proportional to $1/(\text{timespan})^4$, and therefore we expect an increase in sensitivity of about 16 over the KTR94 results.

First, in §2 we describe the 3 different sets of observations that have gone into calculating the limits presented in this article. In §4 we connect the three data sets. In §5 we show the calculation of the new gravitational wave limit. §6 compares the precision of pulsar clocks to those of atomic time standards. §7 is an update of the relationship between \dot{P} and timing noise presented by Arzoumanian et al. (1994). In §8 we discuss the possibility that a planet orbits pulsar PSR B1937+21. Finally in §10 we present our conclusions.

2. Observations

At the NRAO¹ 140-foot (42.7 m) telescope we observed PSR J1713+0747, PSR B1855+09, and PSR B1937+21 in

¹ The National Radio Astronomy Observatory (NRAO) is operated by Associated Universities, Inc., under contract with the National Science Foundation.

addition to others 4-6 times per year at radio frequencies near 800 and 1400 MHz from 1989 October to 1999 July. For details on the analysis of these data see the report by Backer et al. (1993) on results from the first half of the data set. Observations of PSR J1713+0747 started after its discovery in 1994 (Camilo, Thorsett, & Kulkarni, 1994).

We have been conducting monthly observations at 0.43 GHz, 1.4 GHz and 2.4 GHz of an array of MSPs using the NAIC² Arecibo Observatory 300 m telescope since December 1997. These data are used to make precision arrival time measurements for a variety of astrophysical goals. We used the Arecibo-Berkeley Pulsar Processor (ABPP), which is a multi-channel, coherent dispersion removal processor³ with 112-MHz total bandwidth capability (For a detailed technical description of the hardware see Backer et al.(1997.) For PSRs J1713+0747 and B1855+09 we use 56-MHz bandwidth for observations at 1.4 GHz, and 112-MHz for 2.4 GHz, while for PSR B1937+21 we use 45-MHz bandwidth at 1.4 GHz and 56-MHz at 2.4 GHz.

Calibrated total intensity profiles were formed from signals with orthogonal circular polarization. The profiles were then cross correlated with a template to measure times of arrival (TOAs) relative to the observatory atomic clock. Small errors in the observatory UTC clock, of order 1 μ s, were corrected based on comparison of local time to transmissions from the Global Positioning System of satellites (GPS). The templates used for cross correlations were constructed by fitting a set of Gaussian components to long-term averages of observations, using the software described in Kramer et al. (1994) and Kramer (1994). This model fitting scheme is described extensively in Lommen (2001). We use the model to generate noise-free templates with a specific common fiducial point at all frequencies. Lommen (2001) shows that the templates generated in this manner have at most 2 μ s of error in the fiducial point between 1400 and 2380 MHz.

In addition to the two data sets mentioned above, we also have incorporated the archival Arecibo data from KTR94 on PSR B1855+09 and B1937+21 into our analysis. See the original paper for details on these data.

3. Analysis

As we just mentioned, TOAs are calculated via cross-correlation with a template. Before these TOAs can be analyzed several corrections are required:

$$TOA' = TOA + \Delta_{clock} + \Delta_{DM} + \Delta_{backend}$$

Δ_{clock} is comprised of a number of clock corrections which in our case transform a TOA which is referenced against

² The National Astronomy and Ionosphere Center Arecibo Observatory is operated by Cornell University under contract with the National Science Foundation.

³ ‘coherent’ means that the dispersion is removed in the voltage domain prior to power detection.

an observatory maser, to one which is referenced against UTC. Δ_{DM} causes TOA' to be the time that the pulse would have arrived had it been at infinite frequency (lower frequencies are delayed more by the ISM). $\Delta_{backend}$ corrects for any delays that are dependent on the observing backend used. In our case we have a digital latency which is dependent on channel bandwidth and a mid-scan correction which is a result of our on-line folding. After all of these corrections, TOA' is independent of observatory clock, frequency, and observing backend. TOA' marks the space-time event of the arrival of a defined fiducial point of the pulse at the telescope on a defined time scale.

4. Connection of Data Sets

In the TEMPO analysis arrival time of pulses at the observatory is referred to that at the barycenter of the solar system. The solar time corresponding to the rotation of the earth is known as UT1. UT1 is tabulated by measuring the difference between UT1 and UTC. UTC is a solar time scale that runs at the rate of TAI, international atomic time. BIPM tables of (UT1-UTC) are used to orient the observatory in inertial space and make the translation from observatory to earth-center. (UT1-UTC) is between 7 and 32 seconds over the course of our observations, and is known to 0.1 ms at all times. This translates to an uncertainty in TOA of only ~ 0.1 ns. To calculate the earth's position TEMPO uses standard JPL ephemerides DE405.1950.2050. We know the geodetic position of each observatory to within meters. The delays that remain, that are most difficult to account for, are the delays between the arrival of the pulse at the fiducial point of the antenna as defined by VLBI coordinates and the completion of its transmission through the ‘back-end’ of the receiving system. These are typically in the range of 100-3500 ns. At Arecibo, for example, we know that the travel time for a signal from the control room to the Gregorian receivers and back is approximately 7 μ s⁴ largely resulting from the ~ 1200 ft of fiber-optic cabling through which the signal must travel from the platform to the control room. This would give us a ~ 3.5 μ s delay in the TOAs. Typically, we ignore these delays because we take data from a single observatory, with a single operating system, and any constant delay such as this is seemingly irrelevant.

However, these delays become important for connecting multi-observatory data sets. If all such delays at all observatories engaged in pulsar timing were known, it would be possible to have a “Universal Pulsar Timing Array (UPTA)” in which all TOAs from all pulsar data from all over the world could be combined a priori in single meaningful data base. This would necessitate the need for uniform template fiducial point processing. For example, if the world's pulsar astronomers could piece together 17-year data sets on 10 different MSPs with comparable pre-

⁴ Mike Nolan, private communication, 2001 Aug 19

Table 1. Offsets, in μs , between data sets.

Pulsar	KTR94-GB ^a	GB-ABPP ^b
J1713+0747	...	-3.2
B1855+09	-56.9	1.4
B1937+21	-14.4	-0.12

^a GB=Green Bank data^b ABPP=ABPP data (post-upgrade Arecibo)

cision, the sensitivity of the UPTA would go down by a factor of $1/\sqrt{10}$.

In our comparatively small experiment, we attempt this, but can only account for everything but the final 15-60 μs , and so in the end we end up doing a bootstrap connection. We have 3 overlapping data sets. For each pulsar, the average separation between two overlapping sections is used as the offset between the two data sets. These offsets, which will be included in the ITOA format that we will make publicly available, are shown for each pulsar and for each adjacent data set in Table 1. In the case of the Green Bank and ABPP data sets, the TOAs were generated using the same series of Gaussians with the same fiducial point, so all template discrepancies are removed to within 2 μs (see Lommen 2001 for more on this subject). 2 μs in fact, represents the maximum error in going between 1400 and 2380 MHz. The data we have connected is centered from 1330 MHz to 1420 MHz, and the error roughly scales with the size of the bandwidth over which one must construct templates (see Lommen 2001). Therefore the maximum error in connecting our range of data, due to our template cross-correlation is roughly a tenth of 2 μs , or 0.2 μs . In the case of the offset between the KTR94 data sets and the Green Bank data sets, we added, a priori, an amount of offset corresponding to the difference between our fiducial point and the fiducial point of KTR94, who used the peak of the template. These a priori numbers were a phase of 0.443259 for B1855+09 and 0.353460 for B1937+21. The numbers shown in the table, are the offsets in addition to these template offsets. The sign of the offsets are meaningful, e.g. the numbers under the column ‘‘GB-ABPP’’ are the quantities acquired from subtracting the average ABPP residual from the average Green Bank residual during the epoch while they overlap. The offsets between data sets that we processed ourselves (GB - ABPP) are all less than 8 μs .

In order to perform a weighted fit across multiple data sets, it is necessary to be very careful of the average weighting of one data set relative to another. Said another way, with a single set of data, all taken with a single observing system and analyzed uniformly, one need not worry about, for example, overestimating all the error bars by a factor of 3. However, when one is combining two such data sets, if one has overestimated error bars, and a second has underestimated error bars, the fit will

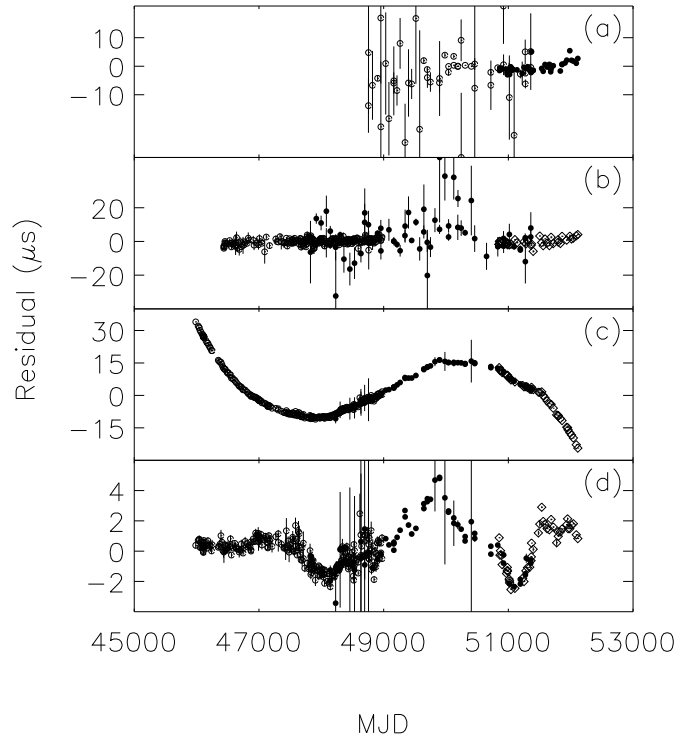


Fig. 1. (a) PSR J1713+0747, (b) PSR B1855+09, (c) PSR B1937+21 and (d) PSR B1937+21 fit for \dot{P} . The open circles are KTR94 data, the filled circles are Green Bank data, and the open diamonds are ABPP data.

tremendously favor the latter. In order to account for this problem, we normalized the error bars in each data set by the total variance per day in those data, i.e.

$$\sigma_{\text{normalized}} = \sigma_{\text{original}} \times \frac{\sqrt{\sum_i 1/\text{err}_i^2}}{L}$$

where L is the length of the data set, in days, and σ_{original} are the error bars that were published by KTR or calculated by us, using the method created by Christophe Lange (private communication) which was adapted from Downs & Reichley (1983).

We used the standard TEMPO package⁵ to perform weighted fits to α , δ , μ_α , μ_δ , P , and \dot{P} , in each of the 3 pulsars. Additionally in J1713+0747 and B1855+09 we fit for the 5 Keplerian parameters and the Shapiro delay parameters, m_2 and $\sin i$ (See Stairs, 1998 for an excellent summary of the process of fitting for the Shapiro delay).

We show the resulting residuals in Figure 1. In (a), (b), and (c), we show J1713+0747, B1855+09, and B1937+21, respectively, fitted for the parameters not marked with footnote ‘‘c’’ in the table. Additionally, in panel (d), we show B1937+21 fitted for $\dot{P}(\dot{\nu})$.

⁵ <http://pulsar.princeton.edu/tempo>

In the next three sections, we discuss various implications of the residuals resulting from these fits. First, we assume the residuals shown in Figure 1 are the result of GWs and use them to place new limits on the GWB. Second, we assume the same residuals are the result of timing noise intrinsic to the pulsars, and determine whether these pulsars are more or less noisy than expected based on the characteristics of the population at large. Finally, we consider the possibility that the residuals in B1937+21 are the result of a planet orbiting that body.

5. Limit on Gravitational Radiation

These data, representing a continuous 17-y set, provide a new limit on the level of background gravitational radiation present throughout the galaxy, and ostensibly the universe. In short, we assume that all the observed fluctuations in the timing residuals are due to the stochastic background of gravitational radiation. This yields the maximum possible gravitational wave spectrum present.

To determine the limit they place, we first need to measure the spectrum of fluctuations that we observe in the timing residuals. The process of computing an observed noise spectrum from irregularly sampled data has been given much consideration by previous authors (Groth 1975; Deeter & Boynton 1982; Deeter 1984; Cordes & Downs 1985; KTR94). These authors are particularly concerned with “red” spectrum where imperfect sampling leads to coupling of spectral estimates at low frequency. Deeter (1984) compares the various methods and determines that the method of fitting the data to orthonormal polynomials produces the most meaningful results. We therefore use this method, as did both Stinebring et al. (1990) and KTR94 in previous generations of this experiment.

Stinebring et al. (1990) and KTR94 start with a calculation which shows that the energy density of background gravitational radiation per frequency octave would have a frequency dependency $\propto \nu^{-5}$ and they go about putting limits on that assumed spectrum. We do the same. However, Rajagopal & Romani (1995), Phinney (2001), and Jaffe & Backer (2002) recently show that the energy density per frequency octave would be proportional to $\nu^{-4.3}$ rather than ν^{-5} . Either way, this is steep compared to the intrinsic spectrum observed in young pulsars, and would not change our results significantly.

A series of polynomials, $p_i(t)$ where i is of the set 0, 1, 2, 3 of corresponding order, is generated orthogonally over the sampling of the timing residuals. We started with the following set:

$$p_{j=0,1,2,3}(t) = \sum_{i=0}^j t^i$$

The process of orthogonalization is done via standard Gram Schmidt reduction. A linear combination of the p_i 's

is found which minimizes the quantity

$$\chi^2 = \frac{1}{\sigma^2} \sum_{n=1}^N \left(r(t_n) - \sum_{j=0}^3 C_j p_j(t_n) \right)^2$$

where $r(t_n)$ is the measured residual at time t_n . The first three C_j 's are covariant with the fitting of the phase, period, and period derivative in the pulsar model. C_3 , however, is a measure of the amplitude of the spectral density of the variance in the timing residuals at a frequency corresponding to $1/T$ where T is the length of the data set. $S_m = \langle C_3^2 \rangle$ is the corresponding estimate of the power (variance) contained near frequency $1/T$. In order to sample the spectrum of S_m over multiple frequencies, we divide the data into smaller and smaller subsets in time, by factors of 2. We refer to the divisor as the frequency index. A frequency index of 2 implies the data set was divided in half, and that therefore we are measuring frequencies of $2/T$, or periods of about 8.5 years.

The results of the spectral measurements are shown in the solid line Figure 2 for PSRs J1713+0747, B1855+09, and B1937+21, using the fits corresponding to parts a, b, and c of Figure 1, i.e. fits through $\dot{\nu}$ only. Though this method works well for irregularly sampled data, the value of the S_m s are still dependent on sampling. In order to gauge the extent of this dependence we have simulated data sets of various spectral indices, with the same sampling as the actual data. Randomly distributed Gaussian noise was transformed into the Fourier domain, multiplied by a function with spectral index 0,2,3, or 5, normalized to $1 \mu\text{s}^2 \text{ y}$ at a frequency of 1 y^{-1} , and transformed back to a time series. Once in the time domain, the data were sampled identically to the actual data. 10,000 such realizations were created for each of the 4 spectral indices. The power spectra of each was measured using the method of orthonormal polynomials described above. The results of this analysis are shown in dotted lines in Figure 2 for each of the 4 spectral indices.

The average value of the spectral estimator, S_m , with spectral index 5 represents the estimate of S_m in the presence of a gravitational radiation, $\langle S_m(\Omega_g h^2) \rangle$, where Ω_g is the energy density in GWs, ρ , expressed as a fraction of the closure density, ρ_c of the universe:

$$\Omega_g = \frac{\rho}{\rho_c} = \frac{8\pi G \rho}{3H_o^2}$$

where H_o is the Hubble constant. We generally express Ω_g in terms of h , i.e. $\Omega_g h^2$ where $H_o = 100 h \text{ km s}^{-1} \text{ Mpc}^{-1}$. We need to translate the normalizing amplitude, ($1 \mu\text{s}^2 \text{ y}$ at a frequency of y^{-1}) into a particular value of $\Omega_g h^2$. We use the relationship derived from the definition of Ω_g (from Stinebring et al. 1990)

$$P_g(f) = \frac{H_0^2}{8\pi^4} \Omega_g f^{-5}.$$

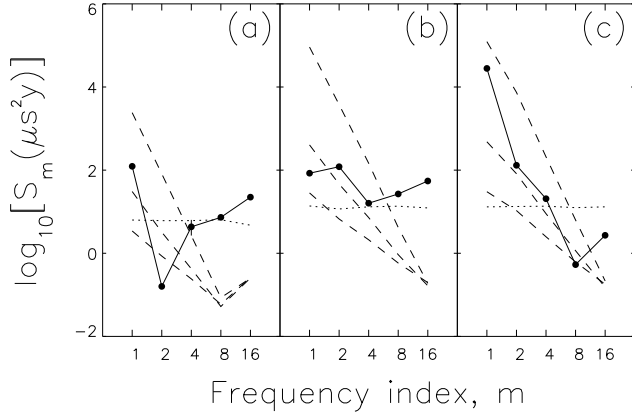


Fig. 2. $\log S_m$ vs frequency index. Solid line shows measured values for each pulsar. Dotted lines show simulated data for spectral index 0. Dashed lines show simulated data for spectral indices 2, 3, and 5. (a) PSR J1713+0747, (b) PSR B1855+09, and (c) PSR B1937+21. Frequencies corresponding to frequency index are m/L where L is the length of the data set: (a) 9.2 yr, (b) 15.6 yr, and (c) 16.8 yr.

where $P_g(f)$ is spectral density, i.e. the same quantity we are attempting to measure with S_m . This means that values of $\langle S_m(\Omega_g h^2) \rangle$ from data with $1 \mu s y$ at a frequency of y^{-1} need to be divided by 752 in order to represent the spectral density when $\Omega_g h^2 = 10^{-7}$ which is the value we represent in Table 2.

Figure 2 shows that the measured spectra of both J1713+0747 and B1855+09 are both quite flat compared to the spectral index 5 model. We would expect J1713+0747 to be somewhat flatter than the others simply by virtue of the plot representing a higher frequency region of the spectrum. PSR B1937+21 demonstrates a steep spectrum, comparable to the spectral index 5 model spectrum, but this may be due to other sources as we will discuss later (e.g. see §8).

In order to calculate the expected influence of gravitational waves on the spectral measurements, S_m , we needed to know the contribution from purely white noise. To this end, we simulated residuals that were only influenced by our known quantities of instrumental noise. We created white noise at the same sampling as that of the three pulsars we are considering. The white data from each observatory were normally distributed random numbers normalized such that their RMS matched the median of instrumental noise from that pulsar at that observatory. The value used for instrumental noise was the standard deviation of the mean of the timing residuals about the mean for a particular day, i.e.

$$stdev = \frac{\sqrt{\sum_i (r_i - u)^2}}{N}$$

Table 2. Observed and computed spectral densities.

Pulsar	m	S_m	$\langle S_m \rangle_w$	$\langle S_m \rangle_g$
J1713+0747	1	348	538	3.21
	2	6.20	435	0.108
	4	22.4	410	3.52×10^{-3}
	8	4.17	420	1.14×10^{-4}
	16	111	278	3.34×10^{-4}
B1855+09	1	84.8	137	121
	2	120	182	5.01
	4	15.6	210	0.195
	8	26.6	204	5.57×10^{-3}
	16	54.7	155	2.51×10^{-4}
B1937+21	1	29379	0.025	164
	2	203	0.028	9.87
	4	11.8	0.035	0.277
	8	7.93	0.035	8.39×10^{-3}
	16	3.43	0.034	2.87×10^{-4}

^a GB=Green Bank data

^b ABPP=ABPP data (post-upgrade Arecibo)

where r_i is a single residual of which there are N averaged to form a daily average and u is the mean of the residuals on that day. We created 10,000 random realizations for each of the 3 pulsars, and measured their spectrum using the same technique shown above. The average value of these data we call $\langle S_m \rangle_w$.

The values of S_m , $\langle S_m \rangle_w$, and $\langle S_m \rangle_g$ for each value of the frequency index, m , are given in Table 2.

In order to attempt to rigorously calculate an upper limit to background gravitational radiation present in our residuals, we duplicate the analysis of Thorsett & Dewey (1996, hereafter TD96). There is significant controversy around this method, which we address following the results. TD96 create a statistic, $Stat_1 = mS_m / [\langle S_m \rangle_w + \langle S_m(\Omega_g h^2) \rangle_g]$, which is normally distributed with m degrees of freedom. The statistic is essentially the measured value of the spectral estimator divided by the predicted value, based on Monte Carlo simulations.

We use a Neyman-Pearson test to determine whether the distribution of $Stat_1$, for various values of $\Omega_g h^2$ is significantly different than the corresponding statistic in the absence of gravitational radiation. The validity of the Neyman-Pearson test is complicated, but it has a simple construction. Consider a particular measurable, A, with probability distribution S1. Correspondingly, consider another measurable, B, with probability distribution S2. The Neyman-Pearson test essentially tests the extent to which the distributions overlap. If they have considerable overlap, they are indistinguishable, if not, they aren't. The quantitative test of 'considerable' involves computing the line which delineates 5% of the area under the curve, representing the least likely outcomes of measuring A. Consider Figure 3 which shows two probability distributions. The area to the left of the dotted line is 5% of the total area

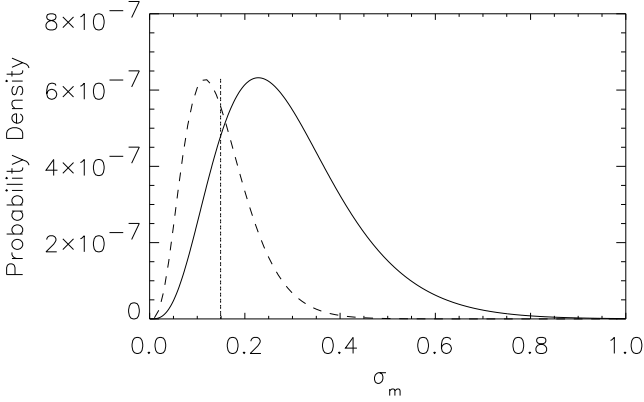


Fig. 3. An example of two different probability density distributions. 5% of the area under the solid curve is to the left of the dotted line.

of the solid curve. The mean value of the dotted curve, falls just to the left of the dotted line. Thus, we can say that these two distributions are different from each other at the 95% confidence level.

One of the subtleties of the Neyman-Pearson test is that one of the two hypothesis is considered the ‘null’ hypothesis, and this is the hypothesis one accepts unless the data compels one to choose otherwise. Thus, the Neyman-Pearson test, by conjecture has a preferred answer, i.e. whatever you choose as the null hypothesis. Our null hypothesis will be that there is no gravitational radiation in the universe. This is of course incorrect. This is the first issue McHugh et al. (1996) have with this method. We are inclined to agree that this is not a good construction.

TD96 used a likelihood ratio, which is an unnecessarily complicated way to construct the Neyman-Pearson test. We merely need to compare the two distributions that are shown in the numerator and the denominator of the ratio TD96 use.

$$S1 = \Pi_{m=1,2,4,8} \chi_m^2 \left(\frac{mS_m}{\langle S_m \rangle_w + \langle S_m(\Omega_g h^2) \rangle_g} \right)$$

$$S0 = \Pi_{m=1,2,4,8} \chi_m^2 \left(\frac{mS_m}{\langle S_m \rangle_w} \right).$$

S0 represents the null statistic, and is shown in the solid line of Figure 4. S1 represents the statistic when a certain amount of gravitational radiation $\Omega_g h^2$ is present. We have plotted S1 in Figure 4 when its value is equal to the 5% limit that we calculate, namely, $\Omega_g h^2 \leq 2.8 \times 10^{-6}$ at a 95% confidence level.

TD96 calculated $\Omega_g h^2 \leq 1.0 \times 10^{-8}$ at a 95% confidence level using only the KTR94 B1855+09 data. Using the technique of TD96 our expanded set of B1855+09 data actually place a weaker limit than the KTR94 data alone, because of the large scatter in the Green Bank data points. The technique separates the data into smaller and smaller

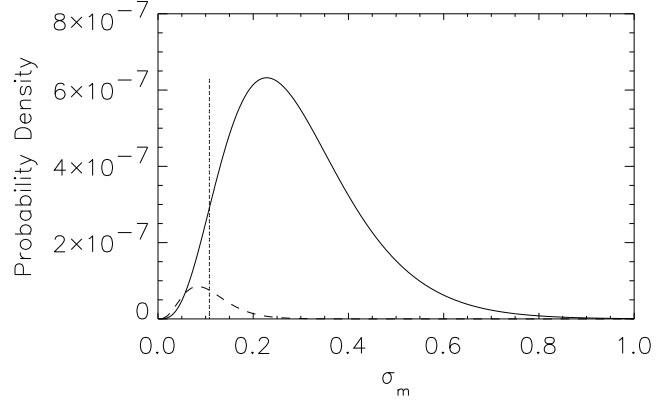


Fig. 4. The solid line shows the probability density of the null statistic, S0, while the dashed curve shows the probability density of the S1 statistic at the 95% confidence value. The dotted line is the same as in Figure 3

sections in order to measure shorter frequencies. The average of these shorter frequency sections is therefore falsely enlarged in our calculations. Using only the $m = 1$ term of our data we have: $\Omega_g h^2 \leq 9.8 \times 10^{-6}$ at a 90% confidence level.

McHugh et al. (1996) rejected the analysis of TD96 because of their use of hypothesis testing rather than parameter estimation. They completed a full Bayesian analysis of the same data which resulted in a much less restrictive limit, $\Omega_g h^2 < 9.3 \times 10^{-8}$, than the analysis of TD96 using the same data.

These opaque calculations cover up the essential nature of the results. After KTR94 we can make a much more simple estimate of the limit these data place on the GWB. We use KTR94 equation 6 which relates the energy density, ρ , in gm cm^{-3} of a gravitational wave to its affect on TOA in μs , A , and a frequency, f , in Hz.

$$\rho = \left(\frac{243\pi^3}{416G} \right) A^2 f^4.$$

The largest amplitude sinusoid that one could conceivably fit to the B1855+09 data has $A = 3 \mu\text{s}$ and $f = 1/17 \text{ yr} = 1.9 \times 10^{-9} \text{ Hz}$. This gives $\rho = 3.2 \times 10^{-38} \text{ gm cm}^{-3}$, or using

$$\frac{\rho}{\rho_c} = \frac{8\pi G \rho}{3H_o^2} = 2 \times 10^{-9} h^{-2},$$

which is more than an order of magnitude smaller than the limit found by KTR94. We assume $H_o = 100 h \text{ km s}^{-1} \text{ Mpc}^{-1}$.

As explained in Lommen & Backer (2001), a gravity wave propagating through the galaxy would have an effect both on the emitting site (the pulsar) and the receiving site (the Earth). Neglecting geometrical considerations for a moment, this could imply that the limit we have just derived will on average be a factor of 2 too high, i.e., that

the response that we see in the pulsar timing, since it results from effects at both sites, is essentially doubled. The factor is not so simple, but depends on (a) the direction of propagation and polarization of the impinging gravitational wave, and (b) the geometrical relationship of the pulsars to the Earth. For a stochastic background of gravitational waves, however, we can calculate the expected effect. If the GW at the emission and reception sites constructively interfere then C_3 will increase by a factor of 2, and S_m will increase by a factor of 4. If emission and reception destructively interfere then S_m will be close to 0 (it will certainly be non-zero due to irregular sampling). The expectation value, i.e. the ensemble average over the 4π directions of propagation, and over the wavelengths in question is a factor of 2, so the limit is actually half what we, or any of these other groups, measure. This of course leaves aside the issue of the variance in the GWB. The background value we measure using these data place a limit on the GWB in a specific place and epoch: in our galaxy and during the 2 decades in which this experiment took place. Jaffe & Backer (2002) are working on a realistic version of the GWB which takes these specifics into account.

We have assumed up until now, that PSR B1855+09 produces the best limit on the GWB since it demonstrates the most stable timing and a long baseline. However, what if there was a geometrical situation in which B1937+21 was experiencing a large perturbation due to GWs while a null occurred at PSRs J1713+0747 and B1855+09? We first need to consider that the limited range of data on J1713+0747 was preventing our detection of any cubic therein. In Figure 5 we performed the same fit that we did for part (c) of Figure 1 but using only the limited range of the J1713+0747 data. The obvious cubic is gone but there is a ‘sawtooth’ present at the level of $2 \mu\text{s}$ that we do not see in the J1713+0747, so we conclude that we are seeing no comparable gravitational wave in J1713+0747.

To attempt to find a geometrical situation which produces an approximate null in J1713+0747 and B1855+09 we inspected the range of possible geometrical multiplicative factors, $(1 - \gamma)/2$ over the 4π sphere of possible gravitational wave directions for each of the three pulsars. See Lommen & Backer (2001) for an explanation of this factor. Figure 6 shows the factor for 2π values of RA while DEC=0° for each of the 3 pulsars. B1937+21 is shown by the solid line. J1713+0747 is the dotted line, and B1855+09 is the dashed line. The three pulsars are close enough together in the sky that $(1 - \gamma)/2$ is highly correlated over the sphere. We chose the DEC=0 line to show because it essentially produces the most favorable spot on the sphere for a B1937+21 gravity wave enhancement with a near-null in J1713+0747 and B1855+09. At DEC=80° J1713+0747 has $(1 - \gamma)/2 = 0.005$, B1855+09 has $(1 - \gamma)/2 = 0.05$, while B1937+21 has $(1 - \gamma)/2 = 0.12$. That gives B1937+21 a $2.4\times$ enhancement over B1855+09 and a $24\times$ enhancement over J1713+0747. The relative

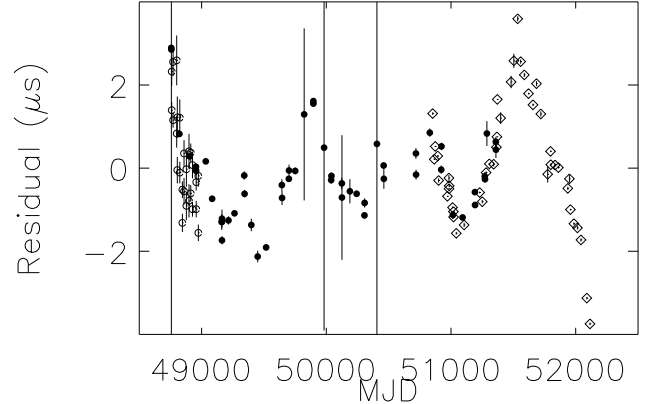


Fig. 5. Residuals from B1937+21 with no $\dot{\nu}$ removed, fitted only to the range of the J1713+0747 data.

strengths of J1713+0747 and B1855+09 can be exchanged somewhat as you can see in Figure 6. We conclude that it would be very difficult to arrange for the ‘deviant’ residuals we see in B1937+21 to be produced by gravitational radiation without producing a similar, but slightly smaller, $\sim 10 \mu\text{s}$ effect, in either J1713+0747 or B1855+09. In addition, a gravitational wave disturbance, which, when reduced by a factor $(1 - \gamma)/2 = 0.12$ still yields a $30 \mu\text{s}$ residual deviation is unrealizable using any known gravitational wave producer in the universe (see Lommen & Backer 2001).

Finally, we consider whether emission and reception site disturbances could be destructively interfering in the case of B1855+09 and constructively interfering in the case of PSR B1937+21. The stochastic GWB can be thought of as ‘crinkled’ space-time. We approximate the crinkling as a sine-wave of equal amplitude but arbitrary phase near each of the 2 pulsars and also near the earth. We begin by computing the enhancement of the amplitude of a sine wave by adding two equal sine-waves together, with a variable displacement, ϕ , between the two. This enhancement we call $E(\phi)$. Thinking of B1937+21 and the earth as emitter and receiver, we may, for example, calculate the probability that $E(\phi)$ will be 5 or greater: 0.001. To obtain the probability that B1937+21’s perturbation will be enhanced over B1855+09’s perturbation by a factor of 25 (roughly the ratio of their peak deviations) or greater we compute the quotient:

$$Q(\Delta\phi) = \frac{E(\phi)}{E(\phi - \Delta\phi)}$$

for $\Delta\phi = [0, 2\pi]$. The probability that $Q(\Delta\phi) > 25$, 0.016, is the probability that the disturbance in B1937+21 is 25 times that in B1855+09. Thus, the residuals we observe in B1855+09 render it highly unlikely that the large amplitude quasi-sinusoid observed in B1937+21 is the result of a GW. Consideration of PSR J1713+0747 would suppress the probability further but not by an equal factor.

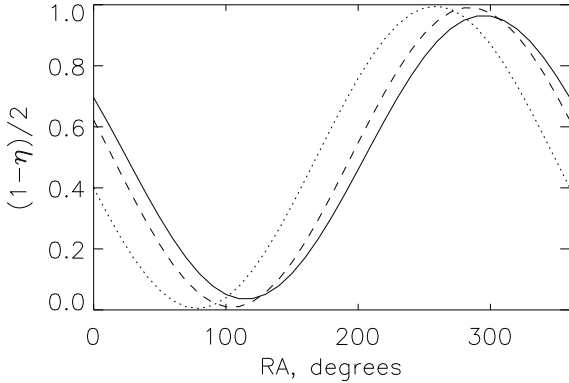


Fig. 6. $(1 - \gamma)/2$ vs RA for DEC=0 for each of the 3 pulsars. B1937+21 is shown by the solid line. J1713+0747 is the dotted line, and B1855+09 is the dashed line.

6. Fractional Stability of Terrestrial Atomic Time Standards vs. Fractional Stability of Neutron Star Rotations

At the baselines considered in this paper, namely longer than 10 years, the fractional stability of neutron star rotations rivals that of terrestrial atomic time standards. To make the comparison quantitative we used the statistic σ_z proposed by Matsakis, Taylor, & Eubanks (1997) for describing pulsar and clock stabilities. The recipe for computing σ_z given in Matsakis, Taylor, & Eubanks (1997) is very complete. We only give a bare outline of the computation process here. We divide the timing residual or clock comparison, $X(t)$, into smaller and smaller subsections of time, starting with the full length, T , and going to $T/2$, $T/4$, $T/8$, etc. To each subset we fit the function

$$X(t) = c_0 + c_1(t - t_0) + c_2(t - t_0)^2 + c_3(t - t_0)^3.$$

σ_z is related to the average of c_3^2 by the following formula

$$\sigma_z(\tau) = \frac{\tau^2}{2\sqrt{5}} \langle c_3^2 \rangle^{1/2}$$

where the angular brackets denote the average, and τ is the length of the subset of data. Figure 7 shows the fraction stability, σ_z vs. dataspan for [UTC-GPS], [TAI-PTB], [TAI-USNO], and [PSR-TAI] for PSRs B1855+09, B1937+21. To compute the error we used the estimate provided by Matsakis, Taylor, & Eubanks (1997), which underestimates the error in the case of data with significant red noise, as is evident in the pulsar data.

Figure 7 shows that PSR B1855+09 beats the [TAI-USNO] time scale at the longest time periods, and is essentially equally as accurate as [TAI-PTB] at timescales of 19 years. Since the fractional stability of B1855+09 improves steadily with increased dataspan, we expect that as additional data on B1855+09 is acquired, this pulsar will easily beat [TAI-PTB] at ~ 25 year timescales unless

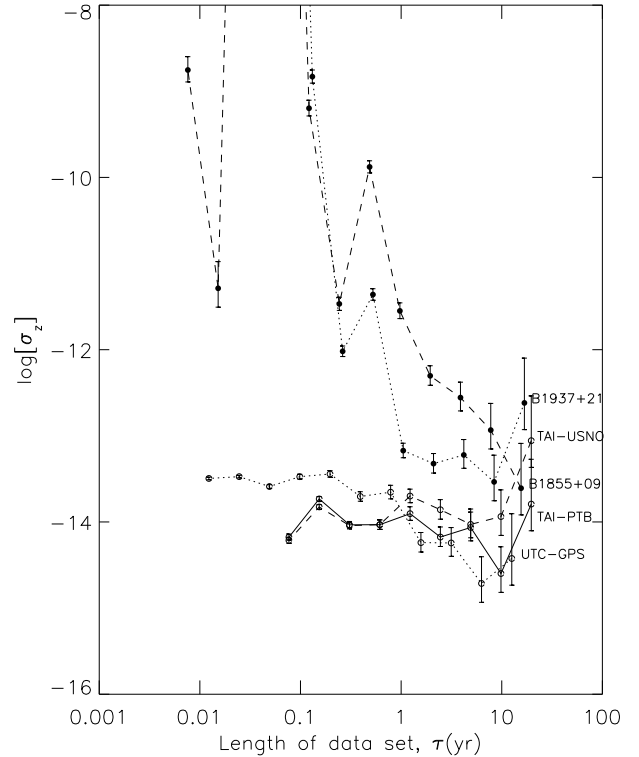


Fig. 7. Fractional Stability of 3 terrestrial timescales, and 2 MSPs.

TAI and PTB improve or the pulsar becomes less stable. Note that TAI is significantly better than USNO alone even though TAI is an aggregate that contains USNO, and similarly, for TT(BIPM) which contains TAI. It is also interesting to note that the PTA allows the possibility of ignoring the earth clock altogether; one degree of freedom in the PTA can be used to solve for time, i.e., PSR vs PSR.

7. Update on Timing Noise as a Function of Period Derivative

Pulsar astronomers have long wondered whether the noise they see in timing residual plots, such as we show in Figure 1 is due to intrinsic instability in the rotation of the pulsar, or is an error in the model, such as a missing planet or unmodeled DM variations. Arzoumanian et al. (1994) published a compendium of measurements of “timing noise” in a number of slow and millisecond pulsars, and suggested that there is a relationship between timing noise and \dot{P} , i.e., the larger the \dot{P} the larger the timing noise. This implies first that the noise is intrinsic to the pulsar, and second that for each pulsar there is a minimum RMS in the residuals that no amount of accounting for systematics will lessen. This has obvious implications for the PTA, and our effort to achieve sub- μ s RMSs on a collection of MSPs. The data presented here along with recently pub-

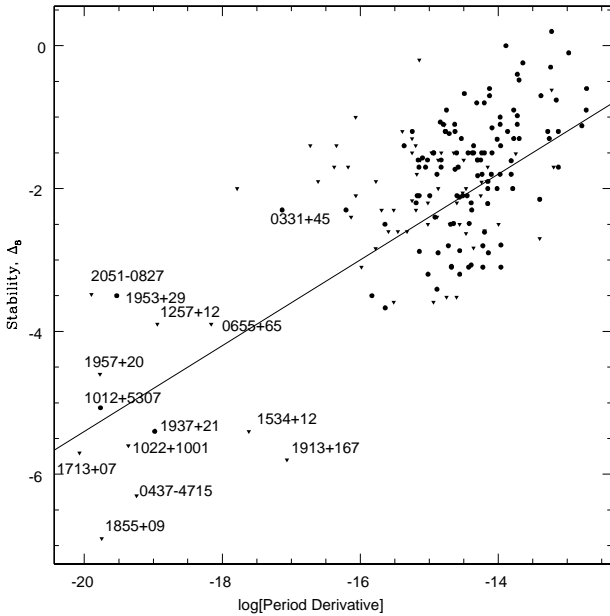


Fig. 8. The timing noise parameter, Δ_8 , as a function of $\log \dot{P}$. Values used are courtesy of Zaven Arzoumanian, except those shown in Table 3, and 1957+20 (Arzoumanian, Fruchter, & Taylor, 1994), B1534+12 (Stairs et al, 1998).

lished results on MSPs allow us to update the picture of timing noise in MSPs as a function of period derivative. This was most recently done by Arzoumanian et al. (1994) who quantified the noisiness of a pulsar using the noise parameter, Δ_8 , defined by

$$\Delta_8 = \log \left(\frac{1}{6\nu} |\dot{\nu}| t^3 \right),$$

where $t = 10^8$ s. Arzoumanian et al. (1994) quote the best fit result to the scatter plot

$$\Delta_8 = 6.6 + 0.6 \log \dot{P}$$

which brought forth the rather depressing notion that we would never achieve better than $1 \mu\text{s}$ accuracy for the MSPs owing to the fact that \dot{P} for the population is $\sim 10^{-20}$ or higher.

We are happy to report that some of the MSPs used to create the low \dot{P} end of the spectrum have been determined to have lower Δ_8 's than were presented in Arzoumanian et al. (1994). We present the new MSP data in Table 3 and the corresponding plot in Figure 8.

The value used for PSR B1937+21 is the best fit to $\dot{\nu}$ letting all the parameters vary. Arzoumanian et al. (1994) were only able to place an upper limit on Δ_8 for PSR B1855+09 and so are we, but ours is significantly lower, -6.9, down from -6. This comes from the best-fit value of $\dot{\nu}$ of $-8 \pm 4 \times 10^{-29}$, where the uncertainty quoted is

that given by TEMPO. This is significantly smaller than the value previously obtained by KTR94, $\dot{\nu} = -1.0 \pm 0.9 \times 10^{-27}$. The value for $\dot{\nu}$ that we use to calculate Δ_8 is different from the value one obtains by only allowing $\dot{\nu}$ to vary. With only 1 degree of freedom, the value is not an appropriate upper limit. For J1713+0747 the fit refines nicely to give $\dot{\nu} = -2.6 \pm 0.2 \times 10^{-27}$.

PSR J0437-4715 was discovered by Johnston et al. (1993). This 5.8-ms pulsar is very bright and has been shown to be very good for timing. The RMS of the residuals, folded and averaged at the binary orbital period, is only 35 ns.

Since a third body was discovered around PSR B1257+12, a new upper limit on $\dot{\nu} < -1.35 \times 10^{-25}$ has been published by Wolszczan et al. (2000). The value is an upper limit since Wolszczan suggests the distinct possibility of a fourth body. While these new measurements do not change the value of Δ_8 significantly from the value reported by Arzoumanian et al. (1994), it is now clear that the value represents an upper limit.

PSR B1534+12 has an updated $\dot{\nu} < 6 \times 10^{-28}$ (I.Stairs, private communication) which yields $\Delta_8 < -5.4$.

PSR B1957+20 is possibly influenced by DM variations, and also by an instable orbital system, as shown by Applegate & Shaham (1994) and Arzoumanian, Fruchter, & Taylor (1994). On the basis of the relationship between DM and RMS DM shown by Backer et al. (1993) we would expect PSR B1957+20, with a DM of 29, to have an RMS DM of about $0.0002 \text{ cm}^{-3}\text{pc}$. We can calculate the expected influence of these DM variations on the estimation of $\dot{\nu}$ which was done on single-frequency data at 430 MHz. A DM of $0.0002 \text{ cm}^{-3}\text{pc}$ corresponds to a timing residual of $5 \mu\text{s}$. A $5 \mu\text{s}$ trend over the course of the observations performed by Arzoumanian, Fruchter, & Taylor (1994) for example, could produce a false $\dot{\nu}$ of $\sim 1 \times 10^{-25}$ given the 5-year observation length. This $\dot{\nu}$ corresponds $\Delta_8 = -4.6$, which is the value attributed to B1957+20 by Arzoumanian et al. (1994). In other words, the timing noise measured by Arzoumanian et al. (1994) could be entirely due to unmodeled DM variations. We therefore make this point an upper limit and emphasize that the true value is probably much smaller.

It seems, then, that a significant fraction of MSPs fall below the line fitted by Arzoumanian et al. (1994). Either the relationship is not well described by a line, or the line has a steeper slope than was published. Either way, this bodes well for the PTA, which relies on submicrosecond accuracy in a handful of pulsars.

Figure 8 is somewhat misleading in that it makes the $\dot{\nu}$ measured in B1937+21 look average. Many of the $\dot{\nu}$'s measured are from single-frequency timing, so DM variations may be contributing to what we are calling 'timing noise.' There is, in fact, no MSP that displays such a convincing, significant $\dot{\nu}$. We measure $\dot{\nu}$ in B1937+21 to 4 significant digits, where as most other MSP measurements are upper limits or at best known to 20%. It is possible that

Table 3. Timing Noise Parameter vs $\ddot{\nu}$ for the MSPs for which they are available.

Pulsar	\dot{P}	$\ddot{\nu}$ (s ⁻³)	Δ_8	Source
J0437+4715	5.72906(5)	$< 5 \times 10^{-28}$	< -6.3	vs ^a
J1012+5307	$1.7134(1) \times 10^{-20}$	$-9.8(2.1) \times 10^{-27}$	-5.1	la ^b
J1022+1001	$4.341(4) \times 10^{-20}$	$< 1 \times 10^{-27}$	< -5.6	kr ^c
B1257+12	$11.4223(7) \times 10^{-20}$	$< -1.35 \pm 0.04 \times 10^{-25}$	< -3.9	wz ^d
J1713+0747	8.54×10^{-19}	$< -2.6 \pm 0.1 \times 10^{-27}$ ^c	-5.6	tw ^e
B1855+09	1.78×10^{-18}	$1 \pm 6 \times 10^{-29}$	< -6.9	tw ^f
B1937+21	1.05×10^{-19}	$1.515 \pm 0.001 \times 10^{-26}$	-5.4	tw ^f
J2051-0827	$1.2737(5) \times 10^{-20}$	$< 2 \times 10^{-26}$	< -3.5	do ^g

^a vs=van Straten et al. (2001) Although van Straten et al. (2001) did not calculate a limit $\ddot{\nu}$ we have estimated this quantity by taking the maximum deviation of their timing residuals (100 ns), converting this to a phase, and dividing by the cube of length of their data set, 3.4 y

^b la=Lange et al. (2001)

^c kr=Kramer et al. (1999) See note above^a. We do the same for this pulsar using 50 μ s and 1700 d.

^d wz=Wolszczan et al. (2000)

^e To calculate an upper limit we have allowed all the other parameters to vary along with $\ddot{\nu}$.

^f tw=this work

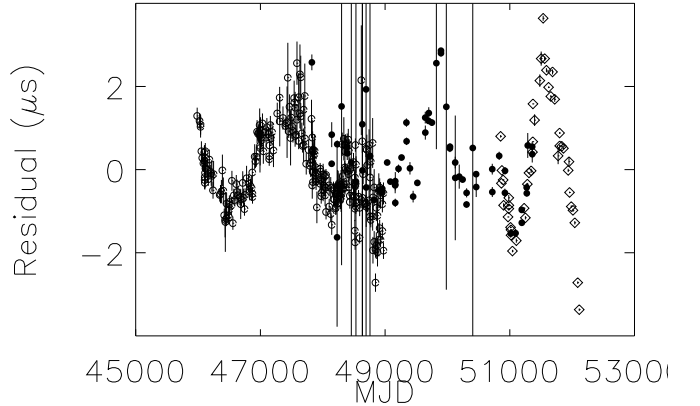
^g do=Doroshenko et al. (2001)

B1937+21 is displaying noise whose source is internal to the neutron star crust. Alternatively, perhaps B1937+21 has a magnetic field structure that is evolving with a 20-y timescale, but we see such evolution at this magnitude in no other object. As an alternative we consider the possibility that B1937+21 is hosting a planet.

8. Planet Around PSR B1937+21?

The residuals shown in part (c) of Figure 1 are the result of a best-fit model α , δ , μ_α , μ_δ , P , and \dot{P} , and includes daily corrections for DM. One possible source of their cubic structure is the existence of a planet of binary period, $P_b = 17.6 \pm 0.2$ y which yields an orbital separation of 8 AU, using Kepler’s Law with a central mass of $1.4 M_\odot$. The residuals after including the planet in the model are shown in Figure 9. $\text{Asin } i$ is $27.1 \pm 0.7 \mu\text{s}$, yielding a companion mass of $0.08 / \sin i M_\oplus$, where i is the inclination of the orbit to the line of sight. If real, this planet would be the smallest known extrasolar planet besides the lunar-mass planet around PSR B1257+12 (Wolszczan et al., 2000). A planet of similar mass ($0.15 / \sin i M_\oplus$) has been found around PSR B1257+12 but is much closer to the pulsar (0.20 AU vs 8 AU) Wolszczan (1994).

The planetary model adds 3 free parameters to the standard fit, T_o , P_b , and $\text{Asin } i$. We compare the goodness of this model to adding the three parameters, $\ddot{\nu}$, $\dot{\nu}$, and $\ddot{\nu}$. The best-fit planetary model fits the data minutely better than the best $\ddot{\nu}$ through $\dot{\nu}$ fit (RMS of $1.14 \mu\text{s}$ vs $1.18 \mu\text{s}$). The best fit parameters are $\ddot{\nu} = 1.07(2) \times 10^{-26} \text{s}^{-3}$, $\dot{\nu} = 1.68(5) \times 10^{-34} \text{s}^{-4}$, and $\ddot{\nu} = -1.42(3) \times 10^{-42} \text{s}^{-5}$. We show in Figure 10 the χ^2 as a function of orbital period, and RMS as a function of orbital period, both of which show a minimum near 17 years, which is the length of our

**Fig. 9.** PSR B1937+21 residuals after fit for a planet.

data set. The dotted line in both parts of the figure shows the value of the quantity when the fit to $\ddot{\nu}$ is turned on instead of the addition of the planet. Only ν , $\dot{\nu}$, T_o , and $\text{Asin } i$ were allowed to vary in the fits. We did not allow α , δ , μ_α and μ_β to vary for consistency with the 2-step fitting process described for B1937+21 in §4.

It is possible that the residuals you see in Figure 1 are the result of some intrinsic property of the pulsar (see §7). For years this pulsar was thought to have significant “timing noise” causing the phase to wander as it does (KTR94). We were concerned that there may always be a well in the figure of χ^2 vs P_b (e.g. Figure 10) where P_b is roughly equal to the length of the data set. We tested this possibility by doing the following. We simulated an extended data set, N years into the future, by assuming that $\ddot{\nu}$ is fixed. We then fit a planet to each data set and looked at the position of the well (in other words, the

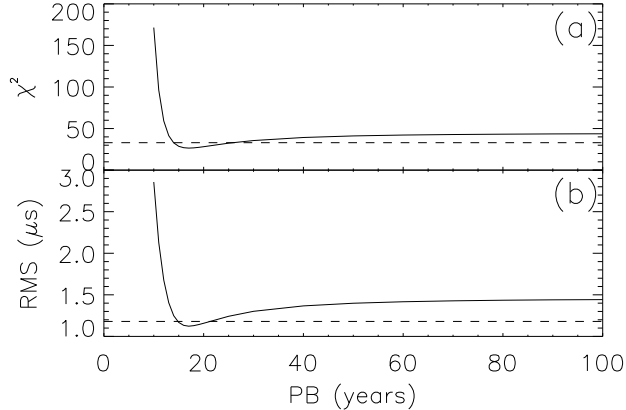


Fig. 10. (a) χ^2 vs orbital period, and (b) RMS vs orbital period for the model using a planet around B1937+21. The dotted line shows the value of the quantity when $\ddot{\nu}$ is used instead.

best-fit P_b) vs N . What we found was that a ‘planet’ will produce a constant $\ddot{\nu}$ up through the year 2020, which is as far as we tested. There is a correlation between orbital period and the length of the data set, as shown in Figure 11. Some of the fits are not stable, such as the point at data span=18 y which yields a 3-y period. Notice that in general, the best-fit planetary orbit is much longer than the data set. This is easily understood if you consider that the planetary model needs to imitate the $\ddot{\nu}$ and can do so by extracting a fraction of an orbit from a putative planet. The non-continuous jumps to a higher P_b shown in Figure 11 are doublings of the orbital period. The χ^2 and RMS for these simulated fits remains very similar to what we observe. We conclude that we could be fooled by a constant $\ddot{\nu}$ into supposing the presence of a planet. However, the previous section, §7, shows that the large and highly significant $\ddot{\nu}$ in B1937+21 is strange relative to the population of MSPs. The only thing that will resolve this is additional ~ 10 years of data, assuming the orbit is about 20 years.

PSR B1937+21 is regarded as having too large a \dot{P} for being a recycled pulsar, i.e. its large \dot{P} alone implies it is a ‘young’ pulsar although it is generally regarded as old Backer et al. (1993). We wondered if perhaps the unknown existence of an orbiting planet could have been skewing the measurement of \dot{P} since the discovery of the pulsar. In fact, it could not. Our best fit \dot{P} without the planet, and without assuming a $\ddot{\nu}$ is slightly smaller, by 1 part in $\sim 10^6$ than our best fit \dot{P} with the planet.

9. Implications of Planet on Possible Evolutionary Scenarios of PSR B1937+21

Millisecond pulsars are thought to be created in supernovae and spun up by accretion from a companion star during the red-giant phase of the companion. Forming

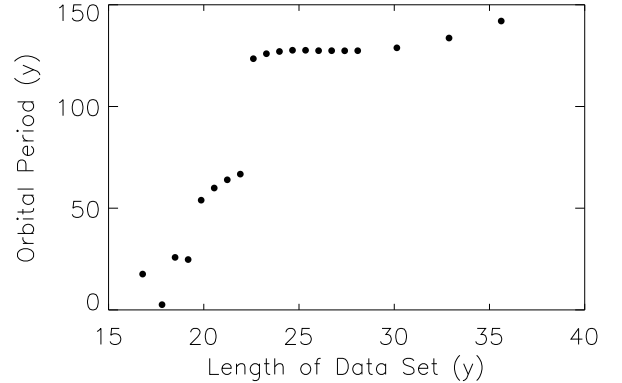


Fig. 11. Best-fit Planetary Orbital Period vs Length of Data Set for simulated extensions of PSR B1937+21 data, assuming a constant $\ddot{\nu}$.

planets around such objects is complex and is the subject of much debate (Wolszczan 1998 and references therein). In fact, finding planets, such as this one, in similar millisecond pulsars helps to solve the mystery in the creation of isolated millisecond pulsars. At the present, of the ~ 70 known millisecond pulsars, 9 are solitary systems, meaning the presence of a companion has not been detected. Given that we suspect these objects have been spun-up by a companion, this presents an inconsistency. However, if planets are somehow the remains of an ablated or otherwise significantly reduced companion, then we would expect to find similar planets around the other 8 known millisecond pulsars. A planet with a 17-y orbit or longer, as we describe would not have been found in any other system, simply by lack of dataspan.

10. Conclusion

We have demonstrated that connection of data sets with sub- μs accuracy across multiple telescopes and many years is possible and yields high precision results for pulsar model parameters. The new limit that our data place on the energy density in background gravitational radiation, $\frac{\rho}{\rho_c} = 2 \times 10^{-9} h^{-2}$, is below that yielded by the work of KTR94 by more than an order of magnitude.

The data suggest the existence of a small ($< 1 M_\oplus$) planet around B1937+21. The best-fit orbital period is currently 17.6 y but that may change with the addition of more data. We have ruled out the possibility that the cubic present in B1937+21’s residuals are due to a GW that has geometrically escaped detection in both J1713+0747 and B1855+09. We also show that if the cubic is due to a $\ddot{\nu}$ intrinsic to the pulsar, that B1937+21 is unique. We find this alternative therefore unlikely.

References

Applegate, J. H., & Shaham, J. 1994, ApJ, 436, 312

- Arzoumanian, Z., Fruchter, A. S., & Taylor, J. H. 1994, *ApJ*, 426, L85
- Arzoumanian, Z., Nice, D. J., Taylor, J. H., & Thorsett, S. E. 1994, *ApJ*, 422, 671
- Backer, D. C., Kulkarni, S. R., & Taylor, J. H. 1983, *Nat*, 301, 314
- Backer, D. C., Hama, S., van Hook, S., & Foster, R. S. 1993, *ApJ*, 404, 636
- Backer, D. C., Dexter, M. R., Zepka, A., Ng, D., Werthimer, D. J., Ray, P. S., & Foster, R. S. 1997, *PASP*, , 109, 61
- Caldwell, R., Kamionkowski, M., & Wadley, L. 1998, *Phys Rev*, D59, 27101
- Camilo, F., Thorsett, S. E., & Kulkarni, S. R. 1994, *ApJ*, 421, L15
- Cordes, J. M., & Downs, G. S. 1985, *ApJS*, 59, 343
- Deeter, J. E. 1984, *ApJ*, 281, 482
- Deeter, J. E., & Boynton, P. E. 1982, *ApJ*, 261, 337
- Doroshenko, O., Lohmer, O., Kramer, M., Jessner, A., Wielebinski, R., Lyne, A. G., & Lange, C. 2001, *A&A*, submitted
- Downs, G. S., & Reichley, P. E. 1983, *ApJS*, 53, 169
- Groth, E. J. 1975, *ApJS*, 29, 443
- Hogan, C. 2000, *Phys. Rev. D.*, 62, 121302
- Jaffe, A., & Backer, D. C. 2002, submitted to *ApJ*
- Johnston, S., Lorimer, D. R., Harrison, P. A., Bailes, M., Lyne, A. G., Bell, J. F., Kaspi, V. M., Manchester, R. N., D'Amico, N., & Nicastro, L. 1993, *Nat*, 361, 613
- Kaspi, V. M., Taylor, J. H., & Ryba, M. F. 1994, *ApJ*, 428, 713
- Kramer, M. 1994, *A&AS*, 107, 527
- Kramer, M., Wielebinski, R., Jessner, A., Gil, J. A., & Seiradakis, J. H. 1994, *A&AS*, 107, 515
- Kramer, M., Xilouris, K. M., Camilo, F., Nice, D. J., Backer, D. C., Lange, C., Lorimer, D. R., Doroshenko, O., & Sallmen, S. 1999, *ApJ*, 520, 324
- Lange, C., Camilo, F., Wex, N., Kramer, M., Backer, D. C., Lyne, A. G., & Doroshenko, O. 2001, *MNRAS*, , 326, 274
- Lommen, A. 2001, PhD Thesis, UC Berkeley
- Lommen, A. N., & Backer, D. C. 2001, *ApJ*, 562, 297
- Maggiore, M. 2000, *Phys. Rep.*, 331, 283
- Matsakis, D. N., Taylor, J. H., & Eubanks, T. M. 1997, *A&A*, 326, 924
- McHugh, M. P., Zalamansky, G., Vernotte, F., & Lantz, E. 1996, *Phys. Rev. D*, 54, 5993
- Phinney, E. 2001, *MNRAS*, submitted, astro-ph, 0108028
- Rajagopal, M., & Romani, R. W. 1995, *ApJ*, 446, 543
- Stairs, I. H., Arzoumanian, Z., Camilo, F., Lyne, A. G., Nice, D. J., Taylor, J. H., Thorsett, S. E., & Wolszczan, A. 1998, *ApJ*, 505, 352
- Stinebring, D. R., Ryba, M. F., Taylor, J. H., & Romani, R. W. 1990, *Physical Review Letters*, 65, 285
- Thorsett, S. E., & Dewey, R. J. 1996, *Phys. Rev. D*, 53, 3468
- van Straten, W., Bailes, M., Britton, M., Kulkarni, S. R., Anderson, S. B., Manchester, R. N., & Sarkissian, J. 2001, *Nat*, 412, 158
- Wolszczan, A. 1994, *Science*, 264, 538
- Wolszczan, A. 1997, In *ASSL Vol. 223: Visual Double Stars : Formation, Dynamics and Evolutionary Tracks*, p. 221
- Wolszczan, A., Hoffman, I. M., Konacki, M., Anderson, S. B., & Xilouris, K. M. 2000, *ApJ*, 540, L41